Separation and Purification Technology 354 (2025) 129101

Contents lists available at ScienceDirect

Separation and Purification Technology

journal homepage: www.elsevier.com/locate/seppur

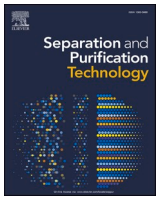

Effect of Li-Na sorbent phase in Ru/Al_2O_3 dual function materials for the Integrated CO_2 capture and methanation

Stefano Cimino [a,*], Elisabetta Maria Cepollaro [a], Francesco Frusteri [b], Luciana Lisi [a]

[a] CNR-STEMS Scienza e Tecnologia per l'Energia e La Mobilità Sostenibili Via G. Marconi 4, 80125 Napoli, Italy
[b] CNR-ITAE Istituto di Tecnologie Avanzate per l'Energia "Nicola Giordano", Via S. Lucia Sopra Contesse, 5, I-98126 Messina, Italy

ARTICLE INFO

Editor: Dr. S Yi

Keywords:
CO_2 Capture and Utilization
Renewable Methane
Chemical Looping
Ruthenium
CO_2 hydrogenation
in-situ DRIFTS

ABSTRACT

The design of highly performing dual functional materials (DFMs) is the key to the successful deployment of Integrated Carbon Capture and Methanation (ICCM) process that combines both steps into a single unit operation with high energy efficiency. Intending to enhance the CO_2 working capacity while preserving high catalytic methanation activity, herein we set out to investigate the effect of combining Li and Na as the CO_2 sorbent phase in Ru/Al_2O_3 DFMs. ICCM tests in a fixed bed reactor operated with alternate feeds indicated that combining Na with Li (or partially substituting it for Li) effectively increases the CO_2 capture capacity and methane production of the DFM. However, this generally requires higher temperatures to properly activate the catalytic methanation and to regenerate the DFM compared to a pure Li-based formulation. Transient operando DRIFTS and catalytic kinetic experiments provided mechanistic insights into the activation/inhibition of different reaction paths on those DFMs containing only Li and/or Na.

1. Introduction

Human-induced CO_2 emissions have been identified as the primary driver of ongoing climate change, prompting an urgent call for innovative strategies to mitigate these impacts. CCU utilizes captured CO_2 to produce value-added chemicals and renewable fuels, offering a promising alternative that extends beyond mere mitigation [1,2]. However, the energy-intensive nature of CO_2 capture and purification processes poses challenges [3]. To address these limitations, an innovative strategy, integrated CO_2 capture and utilization (ICCU), has been proposed which represents a promising platform for green and low-carbon industry transition [2,4–8].

In the ICCU process, captured CO_2 is converted in situ while regenerating the sorbent, eliminating the need for desorption, storage, or purification, resulting in a simplified process and enhanced overall energy efficiency [5–10]. Among the possible alternative routes, the Integrated CO_2 Capture and Methanation (ICCM) using green H_2 has attracted a large interest since methane is a versatile energy carrier that can be seamlessly utilized into existing distribution grids and industrial processes, offering a pragmatic contribution to the gradual transition to a net-zero carbon economy [6–12].

The development of suitable Dual Function Material (DFM) mediators is pivotal to the advancement of such chemical looping processes [7]. These DFMs synergistically integrate CO_2 sorbent phases (e.g., alkali/alkaline earths hydroxides/carbonates) with methanation catalytic active phases (e.g., Ni or Ru) at the nanoscale [5–10]. While Ni-based DFMs offer economic advantages, their sluggish or incomplete reduction during the hydrogenation step at temperatures below 300 °C renders them unsuitable for operation in oxygen-rich environments [5,12,13]. In contrast, Ru-based DFMs, despite their higher cost, exhibit high performance and long-term stability during cyclic operation under representative conditions [9,10,12–18] as well as remarkable self-regeneration capabilities in the presence of sulfur impurities [18], making them the preferred choice for ICCM applications. However, several previous studies have reported that doping Ru-based methanation catalysts with alkali metals such as Na or K at loadings of interest to obtain a reasonable CO_2 capture capacity depresses the intrinsic catalytic activity and CH_4 selectivity [19,20].

The only remarkable exception to this general trend has been reported by our group for Li addition (up to 5 % wt.) to Ru/Al_2O_3 catalysts, which boosts the methanation activity of the supported Ru nanoparticles with fixed dimensions (10–16 nm) [20,21], enabling to limit the loading of the precious metal in the DFM to 1 % wt or lower keeping down the costs. In particular, given the high reactivity of the CO_2 species

* Corresponding author.
E-mail address: stefano.cimino@cnr.it (S. Cimino).

https://doi.org/10.1016/j.seppur.2024.129101
Received 13 May 2024; Received in revised form 23 July 2024; Accepted 3 August 2024
Available online 5 August 2024

preadsorbed over Li-Ru/A, the ICCM process is optimally operated at lower temperatures (260–280 °C) [21,22] when compared to the Na- (310–340 °C) [9,13,15] and Ca- based Ru-DFMs (400 °C) [15,17,23], thus promoting long-term catalyst durability. This is advantageous also considering that CO_2 adsorption on such materials is exothermic and thermodynamically favoured at low temperatures where it still proceeds with fast kinetics [12,14,15,20,22]. Moreover, the Li-Ru/A DFM guarantees roughly 100 % selectivity to CH_4 (negligible CO formation) and an outstanding tolerance to sulfur impurities in the feed [21,22].

However, Li itself is a critical raw material and its unit cost is much higher than Na. As such, the Li loading in the DFM should be kept at a minimum without sacrificing the CO_2 capture capacity of the system or its intrinsic activity, which is of paramount importance to reduce the inventory of materials and make the ICCM profitable [7]. At variance, Li tends to easily react with the support to form bulk mixed aluminates [21,22], which, in turn, can reduce the surface concentration of basic sites available for CO_2 adsorption. Therefore, in this work, we set out to investigate for the first time the effectiveness of combining Li and Na as the CO_2 sorbent elements in Ru/Al_2O_3-based DFMs. In particular, the addition of Na to the sorbent phase (partially replacing Li) is expected to increase the number of weak- and medium-strength basic sites on the DFM [14,15,20], which can enhance the CO_2 capture capacity in an extended temperature range. Moreover, the presence of Li could still promote a fast and complete catalytic conversion of the stored CO_2 into CH_4. Accordingly, the effect of the joint presence of Li and Na on the performance of the cyclic ICCM process was studied in a fixed bed reactor operated isothermally in the temperature range 260 – 400 °C with alternate feed conditions. Transient operando DRIFTS experiments were coupled to catalytic kinetic measurements to evaluate the impact of the two alkali metals on the type of CO_2-derived adsorbed species as well as on the formation of specific reaction intermediate species and possible reaction pathways.

2. Experimental

2.1. Preparation of the DFMs

Ruthenium was preliminarily dispersed (1 % wt. nominal loading) on a commercial γ-Al_2O_3 support (Sasol, 1 mm spherical particles) by an incipient wetness impregnation method using a Ru Nytrosyl Nitrate water solution followed by drying at 120 °C and calcination in air at 350 °C (RuA) [21]. Thereafter, Lithium (1.5 % or 3 % wt.) and then Sodium (3 % wt.) were added in this order by sequential impregnations using appropriate water solutions of their corresponding nitrates followed by drying at 120 °C [18,20]. After each impregnation, the samples were reduced for 2 h under 20 % H_2 /N_2 at 450 °C. Reference DFMs containing only Lithium (3 % wt.) or Sodium (5 % wt.) were also prepared following a similar procedure. DFM samples were labelled *x*NayLi-RuA, with *x* and *y* representing the weight % of alkali. Dispersing Ru first on the support, followed by the alkali metals, ensured consistent dispersion of the precious metal across the DFMs [20,21].

2.2. Characterization of the DFMs

The density of the DFMs was estimated by weighing a known number (80–100) of spheres with a nominally identical volume after stabilization in ambient air for more than 24 h.

N_2 adsorption–desorption measurements at 77 K were performed in a Quantachrome Autosorb 1-C after degassing the DFM samples at 150 °C for 3 h under a high dynamic vacuum. The specific surface area and pore size distribution (PSD) of the DFMs were evaluated by the BET method and the Non-Linear Density Function Theory (NLDFT, cylindrical pore, equilibrium model), respectively. TEM images of the 3Li-Ru/A sample were collected using a transmission electron microscope JEOL JEM-F200 operated at 200 kV and equipped with an EDS probe. The number average size of the supported Ru nanoparticles was calculated based on measurements done using the ImageJ software (80 particles).

X-ray diffraction (XRD) patterns of powdered DFM samples were collected using a Rigaku Miniflex 600 diffractometer with Cu Kα radiation (0.154 nm wavelength) in a 2θ range of 20 – 80°, with a step of 0.01° and 10°/min counting time. Background correction, fitting, deconvolution, and peak attribution were performed using SmartLab Studio II software. The average crystallite sizes of Ru and (Li)Al_2O_3 phases were estimated based on Scherrer's equation from the full width at half maximum (FWHM) of their corresponding main reflections occurring at $2\theta = 43.9°$ [1 0 1] and $2\theta = 66.9°$ [4 4 0], respectively.

A Setaram Labsys Evo TGA-DTA-DSC 1600 flow microbalance was used to measure the CO_2 capture capacity of the DFMs at 30 °C, and to perform temperature-programmed surface reaction tests of preadsorbed CO_2. The DFM sample (90—100 mg) was loaded in an alumina crucible and pre-reduced in situ at 400 °C under a 4.5 % H_2/Ar (70 $cm^3\ min^{-1}$) flow for 1 h; after cooling down under Ar, a stream containing 18 % vol. CO_2 in Ar (70 $cm^3\ min^{-1}$) was introduced for 1 h while monitoring the weight change, followed by purging under 4.5 % H_2/Ar for 25 min. Thereafter, the CO_2-loaded DFM was heated under the same flow up to 700 °C at a rate of 10 °C min^{-1}. The evolved gases were continuously analyzed by a Mass Spectrometer (Pfeiffer Thermostar G) equipped with a Secondary Electron Detector (MS-SEM), recording the temporal profiles at m/z = 2 (H_2), 15 (CH_4), 18 (H_2O), 28 (CO), 44 (CO_2).

Time-resolved-DRIFTS analysis was performed at 280 and 360 °C on powdered DFMs with a Perkin Elmer Spectrum 3 equipped with a liquid-N_2 cooled MCT detector at 4 cm^{-1} resolution. Samples were loaded in a heated chamber equipped with a ZnSe window (PiKe DRIFT) and pre-treated in-situ under 25 % H_2/Ar flow at 360 °C for 1 h. Thereafter, the temperature was set at the desired level and a background spectrum (1 scan) of the reduced DFM was collected under Ar flow before starting the ICCM cycle, which consisted of three sequential steps with alternate feeds and constant total flow rate (15 $cm^3\ min^{-1}$): CO_2 adsorption for 10 min under 15 % CO_2/N_2; purging for 15 min under Ar flow; hydrogenation for 20 min under 25 % H_2/Ar. Spectra (1 scan) were collected every 15 s using Perkin Elmer TimeBase software.

2.3. Integrated CO_2 capture and methanation (ICCM) tests in the fixed bed reactor

Integrated CO_2 capture and methanation tests were performed at atmospheric pressure in a fixed bed reactor (schematically depicted in Figure S1, Supplementary Material) that was loaded with a fixed volume of packed DFM spheres (0.6 cm^3, considering an average void fraction of 39 %) to keep constant the loading of Ru independently from the nature and loading of the alkali metals in each specific sample. Following a reducing pre-treatment in situ at 400 °C under a 20 % H_2/N_2 flow, the DFMs were tested isothermally in the range from 260 to 400 °C, providing alternate feed conditions at a constant total flow rate (20 $Sdm^3\ h^{-1}$) [21]. Specifically, during each test a feed gas stream containing 5 % vol. CO_2 and 0.5 % O_2 in N_2 was stepwise admitted to the reactor and flowed over the DFM for 18 min. The presence of O_2 is important to consider since the catalytic metals can be easily oxidized during adsorption, but they only activate methanation in their reduced form [12]. Thereafter, following a 2 min of purging under pure N_2, the feed was switched to 15 % vol. H_2 in N_2 for a total of 14 min to perform the catalytic methanation of the CO_2 previously captured on the DFM while regenerating the adsorption sites for a new cycle.

A gas analyzer equipped with ND-IR detectors (ABB Optima Advance) was used to continuously measure the molar fractions of CO_2, CH_4, CO. The amounts of CO_2 captured by the DFM and those of CH_4 and CO formed during the hydrogenation phase were calculated by integrating over time their corresponding concentration traces after correction for the gas hold-up in the empty reactor. The overall carbon balance was generally closed within ± 2 %: therefore, the CO_2 conversion and the selectivity to CH_4 were calculated based on the total carbon species released during the catalytic hydrogenation stage. ICCM

performance data were calculated as the average of 3 consecutive repeated cycles (showing a standard deviation below 3 %) excluding the first one at each temperature level.

2.4. Catalytic methanation of gas phase CO_2

Catalytic methanation tests were performed in the same fixed bed quartz reactor by flowing a $CO_2/H_2/N_2 = 1/4/5$ gas mixture over the Na-Li-RuA DFMs (Gas Hourly Space Velocity GHSV=32500 h^{-1}) while heating up the system from 200 °C to 400 °C at ca 3 °C min^{-1} [21]. Before testing the DFMs were reduced in situ at 400 °C under a 20 % H_2/N_2 flow. The rate of the catalytic CO_2 consumption per unit volume of packed-bed DFM (R_vCO_2, [mol s^{-1} dm^{-3}]) was estimated from low conversion data (<10 %) under the assumption of differential conditions, isothermal reactor, and constant molar flow rate. The apparent activation energy for the catalytic CO_2 hydrogenation was calculated from the slope of the corresponding Arrhenius plots. Dedicated experiments were run at fixed temperatures by varying the feed concentration of CO_2 (1.5–10 %vol.) or H_2 (30–50 % vol.) to estimate the orders of the hydrogenation reactions rate (R_vCH_4 and R_vCO) with respect to the partial pressure of each reactant from the plots of ln (R_v) vs. ln (P_{CO2}) and ln (P_{H2}), respectively.

3. Results and discussion

3.1. Characterization of the DFMs

The main results of the textural and structural characterization of the (reduced) DFMs are summarized in Table 1 and Figure 1. XRD in Figure 1a shows diffraction patterns from metal Ru (PDF# 6–666) after the reduction of the DFMs in addition to the signal due to the γ-Al_2O_3 support (PDF# 29–63). Lithium partially reacts with the alumina forming some $LiAl_5O_8$ crystalline phase (PDF# 3–911) [21,22], which keeps the same spinel structure and almost identical lattice parameters. The rest of Li most probably forms an amorphous superficial layer strongly interacting with the support, whose chemical state depends on the environmental conditions [22,24].

The further addition of Na does not alter the XRD patterns, indicating that sodium is well dispersed in an amorphous form on the surface of *x*NayLi-RuA DFMs. The formation of the mixed $LiAl_5O_8$ is accompanied by an increase in the mean crystallite size of the spinel phase (Table 1), which becomes more evident at higher Li loading [22] and upon prolonged exposure to high temperatures. Accordingly, Li addition to the RuA material induces an enlargement of the mean pore size (Figure 1b) from 9.4 nm (characteristic of the commercial alumina spheres [20]) to ca 11 nm, depending on the alkali loading. At variance, the addition of Na to either the RuA or Li-RuA materials does not alter their pore size distribution but only induces a small reduction of the specific surface area due to the proportional increase of density of the DFM spheres (Table 1). It is worth noting that the extensive formation of bulk mixed Li-aluminates can reduce the concentration of those superficial basic Li-sites capable of strongly chemisorb the CO_2.

The crystalline size of Ru in the parent RuA catalyst, calculated using the Scherrer equation, is 10.3 ± 0.7 nm; the presence of Li and/or Na does not modify the characteristic dimension of the metal crystallites in the DFMs (Table 1). TEM images of the 3Li-RuA sample and corresponding EDS maps (Figure 1c-e) show Ru domains with a size distribution centered at ~ 10.4 ± 3.4 nm, consistent with XRD results. However, redox cycles during ICCM testing at temperatures up to 400 °C induced some sintering of the Ru crystallites, whose characteristic size raised up to 16 ± 1.0 nm in the reaction aged 3Na3Li-RuA sample (Table 1).

3.2. CO_2 adsorption and temperature programmed surface reaction with H_2 (H_2-TPSR)

Table 1 reports the maximum weight increase on pre-reduced DFM samples due to CO_2 adsorption (15 % vol.) at 30 °C for 1 h; the corresponding TG temporal traces are presented in Figure 2a.

CO_2 capture occurred rapidly on all DFMs containing either Li or Na or a combination of both as the sorbent phase: the initial weight gain profiles overlapped, thus suggesting that the adsorption process was initially mass-transfer limited by the external transport of CO_2 from the bulk of the gas to the particles within the crucible [22]. The quantity of CO_2 captured in this initial phase (approx. 5 mins) increased along with the total alkali loading in the DFM. Subsequently, CO_2 adsorption continued at a significantly slower rate, requiring almost a hour to approach equilibrium.

Overall, the addition of 3 % wt. Na to the 3Li-RuA DFM proved effective in increasing the CO_2 capacity from 2.63 % wt. up to 3.38 % wt. The CO_2 capacity of the 3Na1.5Li-RuA sample (3.11 %wt.), with half the Li loading, differs by less than 10 %, suggesting that the Na overlayer plays a dominant role in the CO_2 adsorption process on DFMs with mixed alkali metals, due to its lower tendency to form mixed compounds with the alumina support. However, the reference 5Na-RuA sample exhibited a similar CO_2 capacity (3.29 %wt) suggesting a saturation effect at increasing the Na loading. All DFMs spontaneously desorbed similar amounts of weakly bonded CO_2 (approximately 0.4 % wt) during the 20-minute purge at room temperature. In the following H_2-TPSR, all DFMs exhibited an initial weight loss peak at 100–110 °C (Figure 2b), due to the desorption of weakly bonded (physisorbed) CO_2. In line with our previous results [22], methane production was detected from T≥125 °C and it was significantly faster over the 3Li-RuA sample, with an intense peak at approximately 225 °C (Figure 2c) that extended up to ca. 300 °C and was not accompanied by any CO formation (Figure 2d). The addition of Na to the Li-RuA DFM slowed down the surface reaction,

Table 1
Summary of the characterization results for (reduced) DFMs: density of the spheres, Specific surface area (S_{BET}), and pore width by N_2 physisorption; dimensions of Ru (d_{Ru}) and Al_2O_3 (d_{Al2O3}) crystallites from XRD patterns; CO_2 capacity at 30 °C from TGA; apparent activation energy values (E_a) and temperatures for 10 % conversion (T_{10}) for the catalytic hydrogenation of gaseous CO_2.

DFM	Alkali loading		Density	S_{BET}	Pore width (mode)	d_{Ru}	d_{Al2O3}	CO_2 capacity[a]	E_a	T_{10}
	wt %		g cm^{-3}	m^2 g^{-1}	nm	nm	nm	wt %	kJ mol^{-1}	°C
	Na	Li								
RuA	–	–	1.40	180	9.4	10.3	5.5		71	293
5Na-RuA	5	–	1.49	158	9.4	10.7	5.6	3.29	75[b]	
1.5Li-RuA	–	1.5	1.45	158	9.4	11.5	5.6		79	264
3Na1.5Li-RuA	3	1.5	1.55	149	9.4	11.8	6.4	3.11	75	306
3Li-RuA	–	3	1.53	145	10.9	10.6	6.4	2.63	81	265
3Na3Li-RuA	3	3	1.61	138[c]	11.3[c]	16.0[c]	6.9[c]	3.38	75	306

[a] 1h under 19 % vol. CO_2 in Ar.
[b] from ref.[18].
[c] after ICCM testing in the fixed bed reactor (31 cycles) at maximum temperature up to 400 °C.

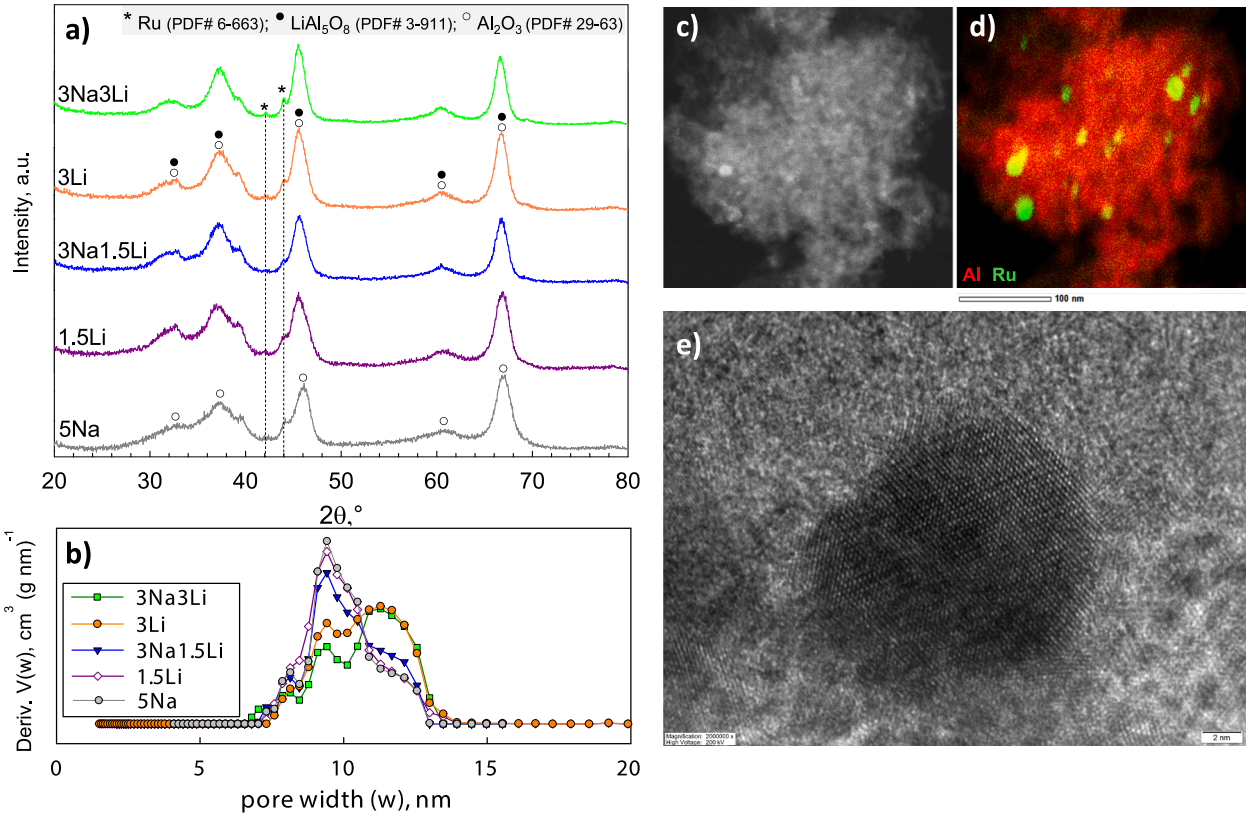

Fig. 1. XRD patterns (a) and Pore Size Distribution (b) analysis (NL-DFT method) of freshly reduced *x*NayLi-RuA DFMs; (c, d) representative TEM image and corresponding EDS map of 3Li-RuA DFM; (e) HRTEM image of a typical Ru nanoparticle on the same DFM.

resulting in methane emission peaks at 265 °C and 275 °C over the 3Na1.5Li-RuA and 3Na3Li-RuA samples, respectively. However, the H_2-TPSR test conducted over the reference 5Na-RuA sample showed that methane production reached a maximum only at 320 °C, a significantly higher temperature which closely aligns with the optimal value reported for the ICCM process over similar Na,Ru-DFMs [10,16]. It follows that a combination of Li and Na can effectively improve the regenerability of the Na-DFM without sacrificing its CO_2 capture capacity. Moreover, the presence of additional CO_2 ad-species more strongly chemisorbed on Na-Al_2O_3 sites expanded the temperature window for methane formation, which extended up to approximately 450 °C. Beyond this temperature, the small amounts of refractory Na-carbonates that were still present on the surface of the sodium-containing DFMs began to react, forming some CO [20], as indicated by the broad emission peaks in Figure 2d extending up to 650 °C.

3.3. *Catalytic activity tests for the methanation of gas phase CO_2*

Catalytic hydrogenation tests of gaseous CO_2 were performed as a sensitive diagnostic tool to investigate the impact of Li and Na + Li addition on the intrinsic activity of the alumina-supported Ru nanoparticles with a fixed characteristic size. Results are presented in Figure 3(a, b) in terms of CO_2 conversion and CH_4 selectivity plots as a function of the reaction temperature; the corresponding Arrhenius plots for the CO_2 consumption rate per unit volume (i.e. at fixed Ru content in the DFM) are reported in Figure 3c. In line with our previous results [21,22], the addition of 1.5 % or 3 % wt. Li to the parent RuA catalyst significantly promoted the catalytic reaction rate by as much as 250 % (at 300 °C), so that the temperature for 10 % conversion (T_{10}, Table 1) was lowered by ca 30 °C down to 265 °C. At the same time, Li-doping on RuA inhibited the formation of CO thus enhancing the process selectivity to methane that closely matched the equilibrium values in the whole range of temperatures explored (Figure 3b). This was accompanied by a modest increase of the apparent activation energy (E_a, Table 1) from 71 to ca 80 kJ/mol. At variance, the further addition of 3 % wt. Na, depressed the methanation activity of the mixed DFMs: T_{10} values for both 3Na1.5Li-RuA and 3Na3Li-RuA increased up to 306 °C implying the specific rate of CO_2 hydrogenation was lowered by a factor of 3.5. The apparent activation energy (75 kJ/mol) was poorly affected up to 285 °C, and corresponds to the values reported for Na-RuA DFMs [18]. Moreover, Na-addition adversely impacted the selectivity to methane, which was always lower than for the parent RuA catalyst: in particular, the selectivity stayed above 90 % up to 285 °C but dropped steeply beyond this temperature down to only 55–60 % at 360 °C (Figure 3b). Since CO is a well-known inhibitor of methanation [25,26] at temperatures up to 350 °C, its increasing partial pressure can progressively impact the CH_4 formation rates by altering the surface coverage on the Ru nanoparticles, specifically decreasing the hydrogen concentration on the metal sites.

Dedicated tests at fixed temperature and low CO_2 conversion (i.e. differential conditions far from equilibrium) were run with 3Li-RuA and 3Na3Li-RuA DFMs to evaluate the apparent orders of the CO_2 reactions leading to either CH_4 and CO (Figure 4). According to its lower intrinsic methanation activity, the 3Na3Li-RuA sample was operated at higher temperatures (ca 40–50 °C) than 3Li-RuA to achieve similar values of CO_2 conversion and it showed CO formation rates almost 2 orders of magnitude larger than its counterpart (Figure 4c,d). Results are also summarized in Table 2: 3Li-RuA displayed average reaction orders of 0.11 and 0.46 for the formation of CH_4 respectively in CO_2 and H_2, which aligns well with previous literature data regarding CO_2 methanation over supported Ru/γ-Al_2O_3 catalysts [27,28]. This suggests that Li-doping does not alter the reaction mechanism but only promotes its rate. At variance, Na-addition markedly decreased the reaction order in CO_2 for the formation of CH_4 making it negative (−0.2), while it roughly doubled the reaction order in H_2 up to 1, which perfectly agrees with recent results for $NaNO_3$ promoted 1 %Ru/Al_2O_3 [27]. The negative CO_2

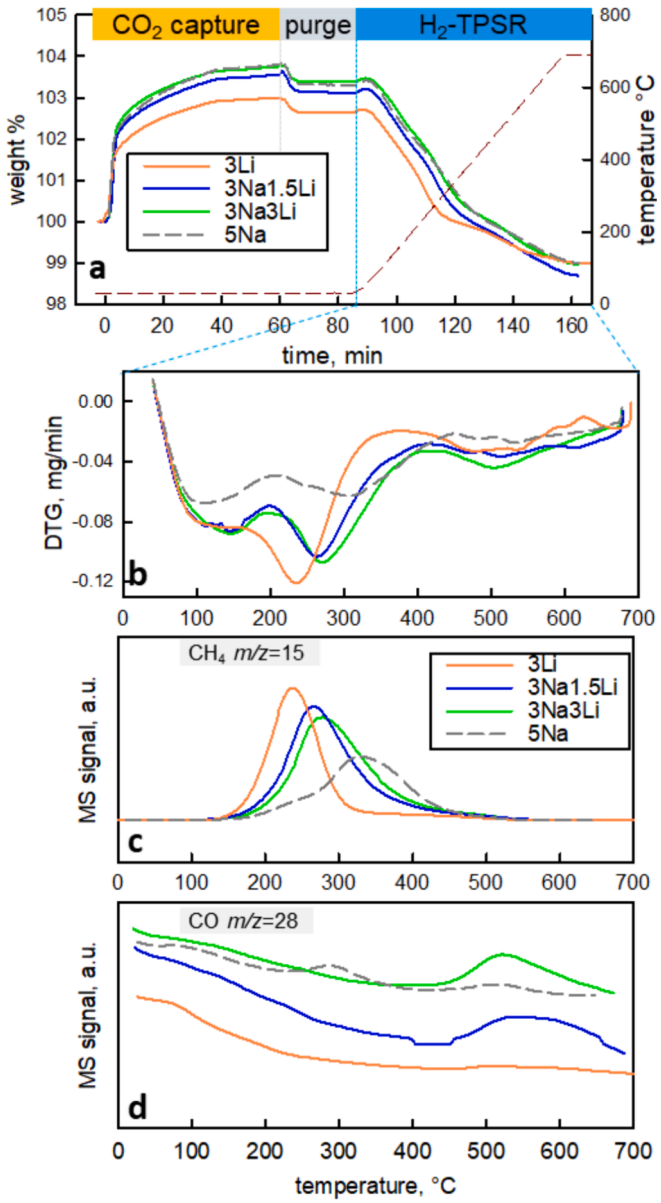

Fig. 2. (a) TG traces recorded during dynamic CO_2 capture tests at 30 °C and subsequent H_2-TPSR experiments on pre-reduced DFMs; (b) corresponding DTG and MS emission profiles for (c) CH_4 and (d) CO as a function of temperature during the H_2-TPSR. Experimental details can be found in Section 2.2.

reaction order implies that Na increases the surface coverage of either CO_2 or CO_2-derived species on the catalytic metal surface, with a consequent decrease of the H* surface coverage, leading to the observed rise in the H_2 reaction order. Since the reaction order for CO formation in CO_2 over 3Na3Li-RuA is approximately 0.3–0.4, it turns out that increasing the CO_2 partial pressure results in a higher CO pressure which can inhibit CH_4 formation. Accordingly, the higher order in H_2 for CH_4 formation over Na-containing DFMs can be also explained considering that a higher H_2 pressure enhances CO removal. It is noteworthy that during the hydrogenation step of the ICCM process, the DFM virtually operates in a CO_2-free environment, contrasting the self-poisoning effect of CO on Ru sites and thus promoting selectivity to CH_4, even with Na-containing DFMs.

3.4. Integrated CO_2 capture and methanation (ICCM) in the fixed bed reactor

CO_2 capture and methanation cycles were run isothermally in the fixed bed reactor loaded with identical volumes of 3Li-RuA, 3Na1.5Li-RuA and 3Na3Li-RuA spheres. The average results of 3 repeated cycles for each temperature level (varied from 240 to 400 °C) are presented in Figure 5 reporting: (a) the amount of the CO_2 captured (i.e. cyclic capacity) and that lost during the intermediate purge phase; (b) the CH_4 produced during the hydrogenation stage; (c) the resulting CO_2 conversion and CH_4 selectivity. In particular, experimental data collected with the 3Li-RuA DFM showed maxima for both the CO_2 capture capacity and methane production (respectively 341 ± 5 and 223 ± 2 μmol cm^{-3} of packed bed, Table 3) when the ICCM cycles were run at 260 – 280 °C, confirming our previous results obtained with the same DFM under identical conditions but for a lower Gas Hourly Space Velocity (8700 vs 32500 h^{-1} in this work) [21].

Operating at higher temperatures progressively affected the CO_2 capacity of the 3Li-RuA DFM, due to the thermodynamic constraints for the exothermic adsorption process [22]. Furthermore, CO_2 conversion decreased slightly from its maximum (93 %) due to an increasing thermal desorption effect driven by the heat released during the methanation stage (Figure S2 and S3, Supplementary Material). Noteworthy, 3Li-RuA formed almost no CO up to 320 °C and its selectivity to CH_4 was still as high as 99 % at 380 °C. On the other hand, for temperatures below 260 °C the catalytic methanation rate was not fast enough to completely regenerate all the CO_2 adsorption sites on the DFM within the time allowed for the hydrogenation step: therefore, the resulting cyclic CO_2 capacity fell below the corresponding maximum adsorption capacity of the DFM at that specific temperature. ICCM results with 3Na1.5Li-RuA indicate that the partial substitution of some of the Li content with Na (1:2 wt ratio) was effective in enhancing the key performance indicators of the DFM (Table 3). In particular, the cyclic CO_2 capture capacity increased up to 320 °C before levelling off up to 400 °C: within this temperature range, 3Na1.5Li-RuA adsorbed as much as 20 % more CO_2 than its 3Li-RuA counterpart. It can be argued that replacing part of the Li with Na provided some additional stronger adsorption sites which require higher temperatures to get activated in the ICCM cycles thus contrasting the typical decline of the capture capacity observed with the 3Li-RuA DFM.

According to the higher stability of CO_2 ad-species on Na-Al sites rather than on Li-Al, the amount of CO_2 spontaneously released from the DFM during the 2 min purge in between capture and reaction stages was reduced by ca 20 % (Figure 5a, Table 3). Operation with 3Na1.5Li-RuA above 260 °C increased CH_4 production giving a maximum value of 259 ± 2 μmol cm^{-3} at slightly higher temperatures (280 – 300 °C), where the CO_2 conversion reached its maximum and the CH_4 selectivity was still above 99.6 % (Table 3). CO formation increased progressively above 300 °C but remained low, thus confirming that the negative impact on the CH_4 selectivity caused by Na (Figure 4) can be effectively suppressed during the ICCM process performing the hydrogenation of pre-adsorbed CO_2 rather than gas phase CO_2. In line with its highest alkali loading, 3Na3Li-RuA outperformed all other DFMs in terms of cyclic CO_2 capture capacity, which progressively increased along with the temperature up to 448 ± 4 μmol cm^{-3} at 400 °C, without showing a definitive approach to the maximum equilibrium level. Methane production followed the same general trend of CO_2 capture, giving a maximum of 322 ± 2 μmol cm^{-3} at as high as 360 °C, where the corresponding CH_4 selectivity was equal to 97.5 % (Table 3).

Temporal traces of the CO_2 concentration during the capture stage at different temperatures (Supplementary Figure S1) confirmed that the adsorption rate was always fast, being mostly completed within 2–3 mins over all the DFMs. Meanwhile, the temperature in the DFM bed increased due to the exotherm released by both the oxidation of the metallic Ru nanoparticles as well as by the CO_2 chemisorption on Li-Al and Na-Al sites. Recalling all tests were run with an identical Ru loading

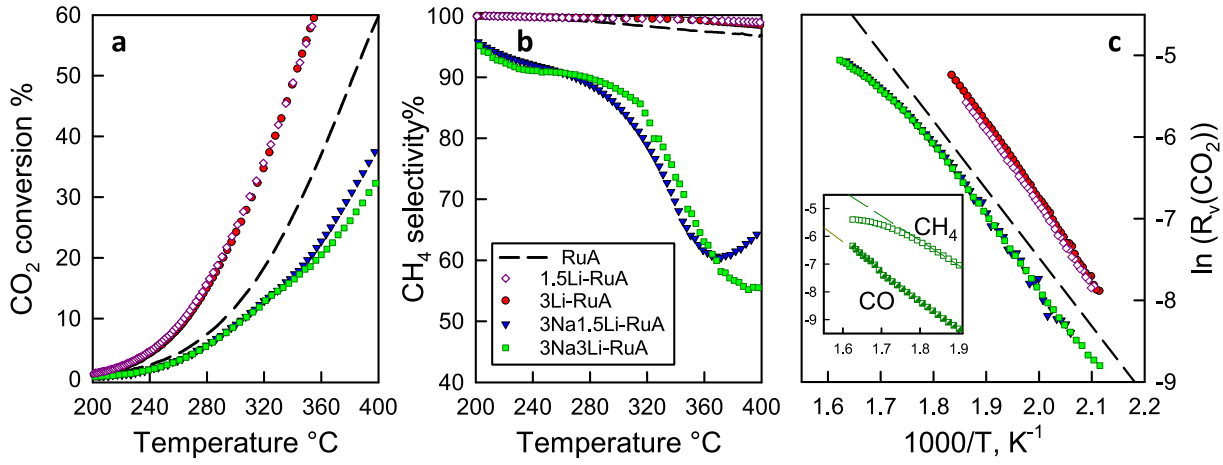

Fig. 3. Catalytic methanation tests of $CO_2 + H_2$ gas mixture over *x*NayLi-RuA DFMs and their parent RuA catalyst: (a) CO_2 conversion, (b) CH_4 selectivity as a function of the reaction temperature and (c) corresponding Arrhenius plots for the CO_2 consumption rate; the inset in panel (c) reports Arrhenius plots for the formation rates of CH_4 and CO over 3Na3Li-RuA. Feed composition: $CO_2/H_2/N_2 = 1/4/5$, GHSV=32500 h^{-1}. Experimental details can be found in Section 2.4.

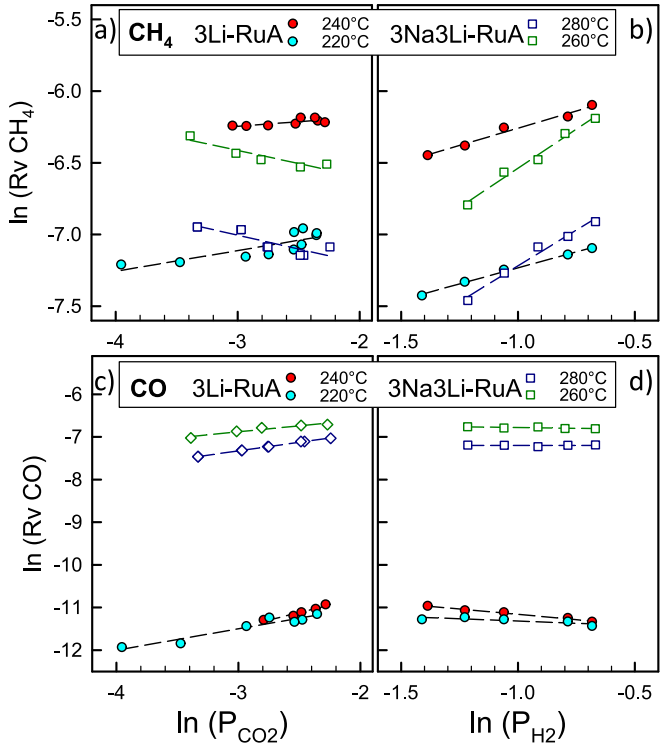

Fig. 4. Effect of the partial pressures of CO_2 and H_2 on the catalytic formation rates of CH_4 and CO during the hydrogenation of $CO_2 + H_2$ gas mixtures over 3Li-RuA and 3Na3Li-RuA DFMs at different temperature levels. Experimental details can be found in Section 2.4.

Table 2
Apparent orders of reaction for the formation of CH_4 and CO in CO_2 (n1, n2) and H_2 (m1, m2) over 3Li-RuA and 3Na3Li-RuA at two temperature levels.

DFM	Temp. °C	$R_v(CH_4) = k_1 P_{CO2}^{n1} P_{H2}^{m1}$ n1	m1	$R_v(CO) = k_2 P_{CO2}^{n2} P_{H2}^{m2}$ n2	m2
3Li-RuA	220	0.14	0.45	0.50	−0.60
	240	0.08	0.48	0.70	−0.50
3Na3Li-RuA	260	−0.19	1.00	0.38	0.00
	280	−0.18	1.09	0.29	−0.08

in the reactor, the larger temperature rise observed with Na-containing DFMs under conditions of equal CO_2 capture (i.e. at 260 °C) reflects a larger average heat of formation for surface Na-carbonates. It was already observed by H_2-TPSR results that the larger CO_2 capture capacity of Na-containing DFMs cannot be exploited at low temperatures due to kinetic limitations for the catalytic hydrogenation. This also appears when comparing the typical temporal CH_4 flow recorded during the ICCM operation with each DFM at a fixed temperature level (Figure 6 a,b). Even at a low temperature of 260 °C (Figure 6a), methane production started with each DFM as soon as H_2 was admitted to the reactor according to the fast reduction of RuO_x to its active metallic form. However, the methanation of pre-adsorbed CO_2 was faster over 3Li-RuA, producing a sharp CH_4 flow peak (after just 10 sec) whose maximum value was as much as 3.5 and 2.5 times higher than over 3Na3Li-RuA and 3Na1.5Li-RuA, respectively. Thereafter, the reaction rate slowed down due to the progressive consumption of the available CO_2, and its production was mostly concluded within the first 3–4 mins (inset in Figure 6a). At variance, methane formation extended over the entire hydrogenation period with the Na-containing DFMs, eventually resulting in a slightly larger overall production than over the pure Li-counterpart. Increasing the temperature by 100 °C up to 360 °C only doubled the maximum CH_4 flow rate recorded over Na-containing DFMs (Figure 6b,c), indicating a low apparent activation energy for the catalytic hydrogenation of the CO_2 pre-adsorbed on Na-Al sites, which aligns with the results of the gas-phase methanation tests (Figure 3c). Nevertheless, at this higher temperature, it was possible to activate a larger pool of more refractory CO_2-ad species stored on the DFM, which were mostly converted within the first 8–9 min of reaction (inset Figure 6b). At variance, the maximum CH_4 flow measured over 3Li-RuA increased much more steeply with temperature (Figure 6c), roughly doubling from 240 °C to 280 °C, before reaching a plateau at higher temperatures. It is argued that beyond 280 °C the reaction rate over 3Li-RuA was initially controlled by the H_2 mass transfer during its stepwise addition to the reactor, and soon after it dropped due to the lack of (adsorbed) CO_2 to be converted, confirming the absence of residual poorly-reactive carbonates. 3Na1.5Li-RuA provided a slightly higher methanation rate than 3Na3Li-RuA up to 360 °C (Fig. 6c): this agrees with the results of gas-phase catalytic tests and confirms the kinetics of the catalytic hydrogenation reaction were largely controlled by the inhibiting effect of Na, which was slightly stronger in the DFM with larger Li-content. In particular, the sequential addition of Na above Li appears to form an overlayer that partially prevents Li-sites from participating both in the CO_2 capture and the hydrogenation reaction mechanism. Alternative DFM preparation strategies can be envisaged to limit this inhibiting

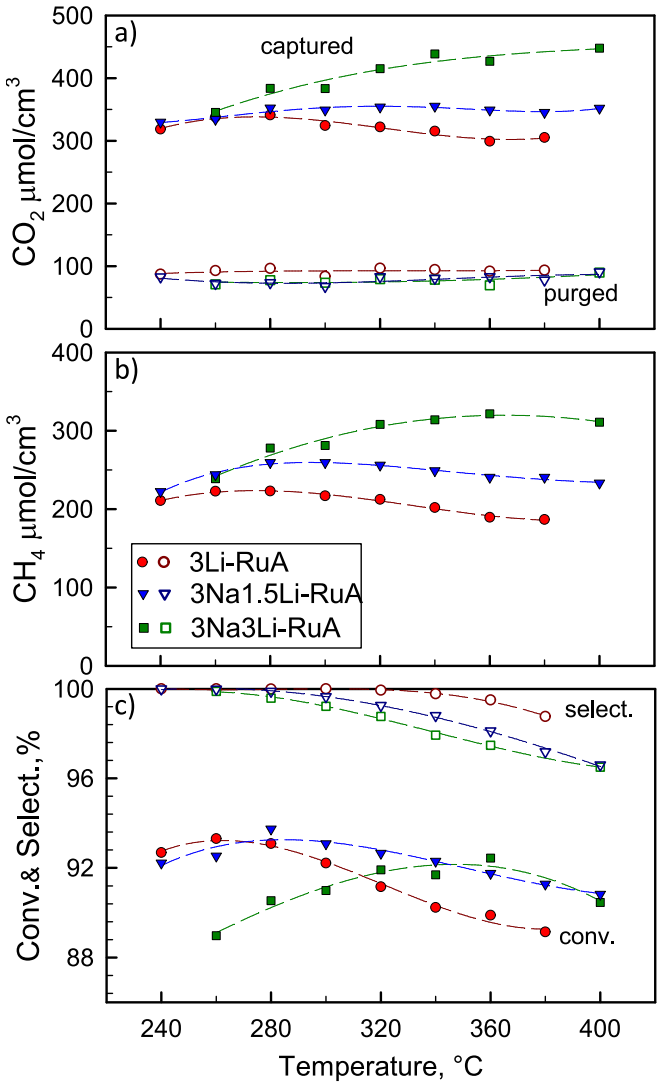

Fig. 5. Effect of the reaction temperature on the average amounts of (a) CO_2 captured and CO_2 desorbed during purging, (b) CH_4 produced, (c) CO_2 conversion and CH_4 selectivity during 3 consecutive cycles of ICCM with 3Li-RuA, 3Na1.5Li-RuA and 3N3Li-RuA DFMs. Feed conditions: adsorption 5% CO_2, 0.5% O_2 in N_2; hydrogenation 15% H_2 in N_2. Experimental details can be found in Section 2.3.

effect of Na by changing the order of deposition of Ru, Li and Na on the alumina support.

Eventually, the same batch of 3Na3Li-RuA DFM completed a total of 31 ICCM cycles during 30 days in the reactor (held at temperatures in the range 260 – 400 °C) without performance degradation: this is evidenced by consistent key process indicators for ICCM tests at 340 °C with the fresh and the reaction-aged DFM (Supplementary Table S1). These findings align with previous reports on Ru-DFMs containing either Li or Na as the sorbent phase, showing long-term stability during cyclic operation under representative conditions at mild temperatures (320 °C) [9,10,12–18]. Specifically, while the reaction-aged 3Na3Li-RuA DFM exhibited a slight increase in Ru crystallite size (Table 1), this did not impact its methanation activity. However, the DFM's durability may be challenged if the ICCM reaction temperature needs to be raised to 400 °C or above to fully utilize the CO_2 capture capacity and boost the methane production rate.

3.5. Time-resolved DRIFTS characterization of the ICCM cycles

Time-resolved DRIFTS experiments were performed to get mechanistic insights into the ICCM cycle over the mixed 3Na3Li-RuA DFM at two different temperature levels (280 °C and 360 °C). Considering recent literature reports suggest minor effects of the presence of O_2 during the CO_2 capture on similar DFMs [18,21,35] and present fixed-bed reactor ICCM tests indicated that RuO_x reduction occurred readily at the beginning of the hydrogenation step without delaying methane formation at each temperature level, DRIFTS experiments were run without oxygen during CO_2 adsorption to simplify data interpretation. Figure 7a shows the temporal evolution of the integrated intensities of the two main bands related to carbonate/bicarbonate/formate species respectively peaking around 1600 cm^{-1} and 1350 cm^{-1}, which were formed and consumed on the surface of the DFM during a representative cycle at the investigated temperatures. The corresponding DRIFTS spectra acquired at four characteristic times during the cycle (labelled t1-t4 in Figure 7a, respectively corresponding to the end of the CO_2 capture and of the purge, the beginning of the hydrogenation step and later on towards its end) are presented in Figures 7b and c for each temperature level.

The two main bands in the region of carbonates (peaking at 1615 cm^{-1} and at 1345–1340 cm^{-1}) can be mostly assigned to chemisorbed bi-dentate carbonates [16,18,22,29,30,31] which were readily formed upon exposure of the pre-reduced DFM to CO_2, thus confirming the fast kinetics of the adsorption process. A shoulder at 1545 cm^{-1}, due to monodentate carbonates [27,32], is also detectable on the main band at high frequency.

The contribution from formate species (HCOO*), which can give several (relatively small) signals in the range from 1750 to 1200 cm^{-1} (mostly at 1720, 1620, 1405, 1390 cm^{-1} [33]) should be also considered. This is confirmed by the coexistence of the unresolved signals in the range from 2850 to 3000 cm^{-1} peaking around 2925 cm^{-1} indicative of the C–H stretching of adsorbed formates (insets in Figs. 7b,c) [33,34] and methylene groups or aliphatic hydrocarbons on the catalyst surface, most probably on the Ru particles [26]. Additionally, physisorbed bicarbonate species (main signals at 1690, 1650 cm^{-1}) were formed more slowly under the CO_2 flow, resulting in the observed progressive increase of the initial $\Delta\nu$ between the two main bands [30,35]. This aligns with the results of TG experiments showing a slower CO_2 adsorption tail taking place after an initial fast CO_2 capture phase lasting

Table 3
Summary of the average results obtained during 3 consecutive runs of ICCM in the fixed bed reactor with DFMs at their optimal operating temperature. Feed sequence and composition: 5 % CO_2, 0.5 % O_2 in N_2 for 18 min; N_2 purge for 2 min; 15 % H_2 in N_2 for 14 min.

DFM	Temp.	CO_2 captured	CO_2 purge	CO_2 desorb.	CH_4 prod.	CO_2 conv.[a]	CH_4 select.[b]
	° C	µmol cm^{-3}				%	
3Li-RuA	280	341	96	17	223	93.1	99.99
		(±5)	(±5)	(±2)	(±2)	(±0.2)	(±0.01)
3Na1.5Li-RuA	300	352	68	19	260	93.1	99.64
		(±6)	(±5)	(±1)	(±2)	(±0.4)	(±0.03)
3Na3Li-RuA	360	427	69	27	322	92.4	97.48
		(±8)	(±3)	(±2)	(±2)	(±0.5)	(±0.14)

[a] $(CH_4 + CO)/(CH_4 + CO + CO_{2\ des})$.
[b] $CH_4/(CH_4 + CO)$.

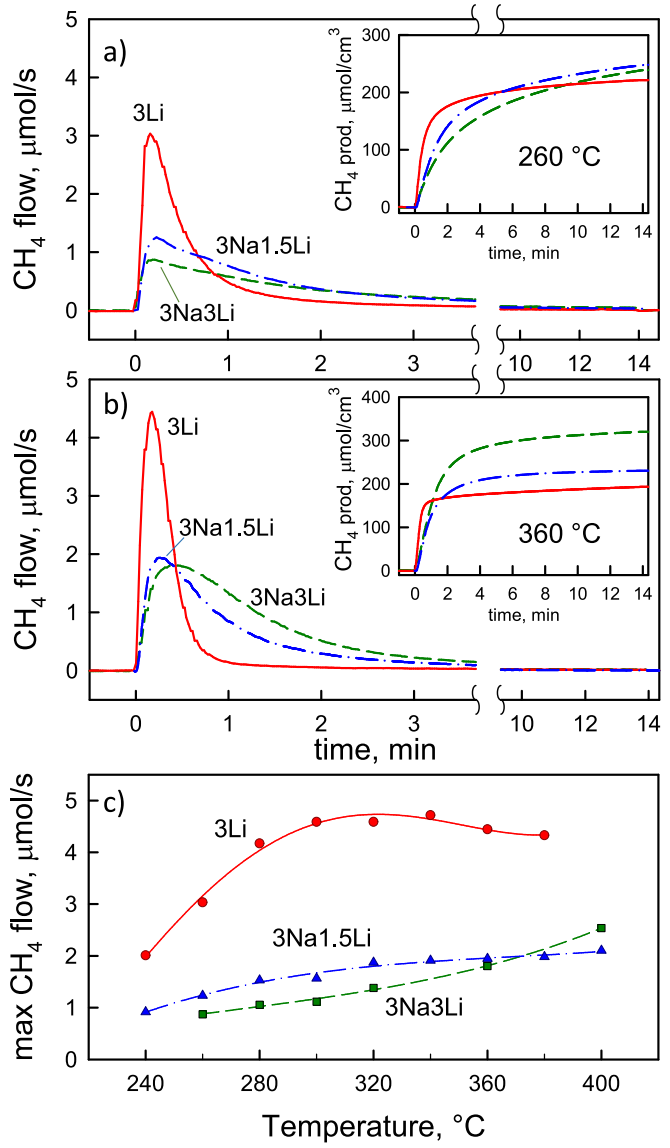

Fig. 6. Temporal evolution of the CH_4 flows produced over 3Li-RuA, 3Na1.5Li-RuA and 3Na3Li-RuA DFMs during the hydrogenation stage following the CO_2 capture performed at (a) 260 °C and (b) 360 °C: the insets report the corresponding cumulative amount of CH_4 produced as a function of time. (c) Effect of the reaction temperature on the maximum CH_4 flow formed over each DFM. Experimental details can be found in Section 2.3.

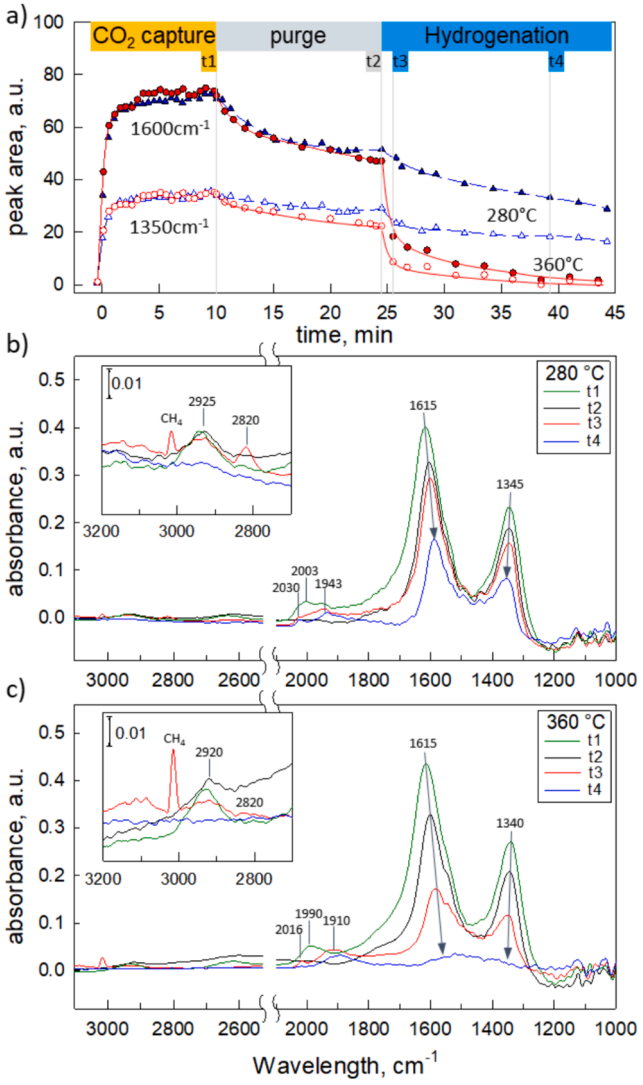

Fig. 7. Time-resolved DRIFT spectra during the ICCM over 3Na3Li-RuA DFM operated at 280 °C and 360 °C. a) Temporal evolution of the integrated areas of the two main carbonate/formate bands on the DFM (blue triangles 280 °C, red circles 360 °C; full symbols 1600 cm^{-1}, empty symbols 1350 cm^{-1}); b, c) DRIFT spectra recorded at each temperature during the ICCM (shown in panel a) at characteristic times: (t1) the end of CO_2 adsorption, (t2) after purging, (t3) after 1 min and (t4) 14 min of methanation. DFM pretreated at 360 °C under 25 % H_2 in Ar. Feed sequence: 15 % CO_2 in N_2, 10 min; inert purge, 15 min; 25 % H_2 in Ar, 20 min. Experimental details can be found in Section 2.2.

about 5 min. Weakly bonded bicarbonates were spontaneously desorbed during purging under inert flow, as confirmed by the (limited) reduction of the peak intensities in Fig. 7a (more evident at higher temperatures) which is mostly due to a loss of contribution from higher wavenumber signals (black spectra @ t2 in Figure 7b,c). At variance, adsorbed formate species were rather stable upon purging, as shown by the corresponding signal at 2925 cm^{-1}, which persisted unchanged at the end of this phase at 280 °C (and was only slightly affected at 360 °C).

Interestingly, the overall amount of adsorbed carbonaceous species formed on the 3Na3Li-RuA DFM (pre-reduced at 360 °C) under the CO_2 flow was poorly affected by the temperature of the cyclic process (Fig. 7a).

During CO_2 adsorption at 280 °C, in the region of the surface carbonyls, a main broad band appeared at 2003 cm^{-1} with a shoulder at 2030 cm^{-1}, which can be assigned to CO* linearly bonded on Ru^0 [33]. The additional signals detected at 1943 cm^{-1} extending down to ca 1800 cm^{-1} correspond to bridged carbonyls between two or more Ru atoms [26,33]. Increasing the temperature up to 360 °C had a minor impact on the formation of bridged carbonyls in the wide envelope ranging from 1980 – 1800 cm^{-1}, while the feature at 2030 cm^{-1} due to linear CO* on Ru disappeared [16,27,36–38]. Regardless of the operating temperature, carbonyl species formed during CO_2 adsorption were mostly removed by the purge as shown by the flat spectra acquired in the corresponding region at the end of this phase (black lines in Fig 7b,c).

Soon after H_2 was admitted to the DRIFTS cell, the intensities of the carbonate bands started to decrease indicating these species were consumed to form methane. Accordingly, a sharp band at 3015 cm^{-1} appeared at the beginning of the hydrogenation step (@t3: red spectra in Fig 7b,c and corresponding insets) mirroring the initial release of gaseous methane (more intense at 360 °C) that progressively reduced and vanished for longer times on stream (blue spectra @t4). In line with the ICCM results in the fixed bed reactor, the methanation proceeded at a much faster rate at 360 °C than at 280 °C and completely consumed all the adsorbed carbonates (Fig. 7a) and formates (insets in Fig.7c) during

the first 10 min. At variance, the residual presence of unreacted adsorbed carbonates at lower temperatures ultimately limited the cyclic CO_2 capacity of the DFM. At the beginning of the hydrogenation at both temperatures, those bands in the region 1840–1950 cm^{-1} due to bridged carbonyls reappeared accompanied by smaller bands due to linear carbonyls peaking at 2016 and 2030 cm^{-1} at 360 and 280 °C respectively: overall Ru-carbonyls went through a maximum at the beginning of the hydrogenation step (t3) while bridged-CO* and, to a lower extent, linear CO* persisted on Ru (with reduced intensity) at the end of the hydrogenation period (t4).

Moreover, a novel band appeared at 2820 cm^{-1} during the reaction at 280 °C (less evident at 360 °C) and it followed the same temporal evolution of methane (insets of Fig 7b,c): this signal can be assigned to C–H vibrations of methoxy groups, which are possible intermediates in the conversion of formates to methane at the metal-support interface [34,38,39].

Eventually, DRIFTS experiments were repeated over the reference DFMs containing only Li or Na (3Li-RuA and 5Na-RuA) to highlight specific effects due to each alkali. The corresponding spectra acquired at the same characteristic times during cyclic operation at 280 °C are shown in Figure 8 (a,b) together with a simplified schematic representation of the main surface species detected over each DFM.

While bidentate carbonates represented the most abundant adsorbed species over either Li- and Na- DFMs, sodium was also responsible for a larger formation of monodentate carbonates giving the characteristic shoulder band at ca 1550 cm^{-1}: this was also detected over the mixed 3Na3Li-RuA sample, but barely visible over 3Li-RuA. Analogously, the presence of Na led to a significant formation of formate species at the interface with Ru (C–H stretching band at 2920 cm^{-1}), which, at variance, were substantially absent at the interface between Li and Ru (insets in Figure 8). A striking difference between Li- and Na- DFMs was represented by the type (and amount) of carbonyl species formed on Ru^0 upon CO_2 adsorption. In the case of Li-Ru, DRIFTS revealed only the band at 1840 cm^{-1} assigned to multi-bridged carbonyl species on the metal nanoparticles, which, in turn displayed a quite low overall coverage of C-species. On the other hand, when in contact with Na, the Ru surface ended up largely covered by different types of linear CO* species (bands at 2028, 1992 cm^{-1}) as well as bridged (1943 cm^{-1}) and possibly multi-bridged carbonyls. During the subsequent hydrogenation step, the low C-coverage of Ru in contact with Li favoured the dissociative adsorption of H_2, which, in turn, can convert those stored bidentate carbonates into CH_4 via the transient formation of novel bridged carbonyls (band at 1945 cm^{-1}) as the key intermediate species [24]. At variance, more linear and bridged carbonyl species (bands at 2028, 1992, 1945 cm^{-1}) as well as formates (2920 cm^{-1}) populate the Ru surface in contact with Na, causing site blocking/poisoning for H_2 adsorption, and a consequent shortage of H* [28]. In this case, the transient appearance of methoxy intermediates (band at 2790 cm^{-1}) was possibly related to the conversion of formates at the Na-Ru interface to methane. The lack of H* availability on the metal sites is the cause of the slower kinetics for this reaction path at any temperature (Figure 6).

Interestingly, recent SSITKA/DRIFTS results during the standard methanation reaction (i.e. co-feeding CO_2 and H_2) over Ru/Al_2O_3 catalysts and Na-promoted counterparts [27] confirmed that sodium changes the reaction mechanism. For the unpromoted Ru/Al_2O_3 catalyst only bicarbonate and carbonyl species [38] were identified as reaction

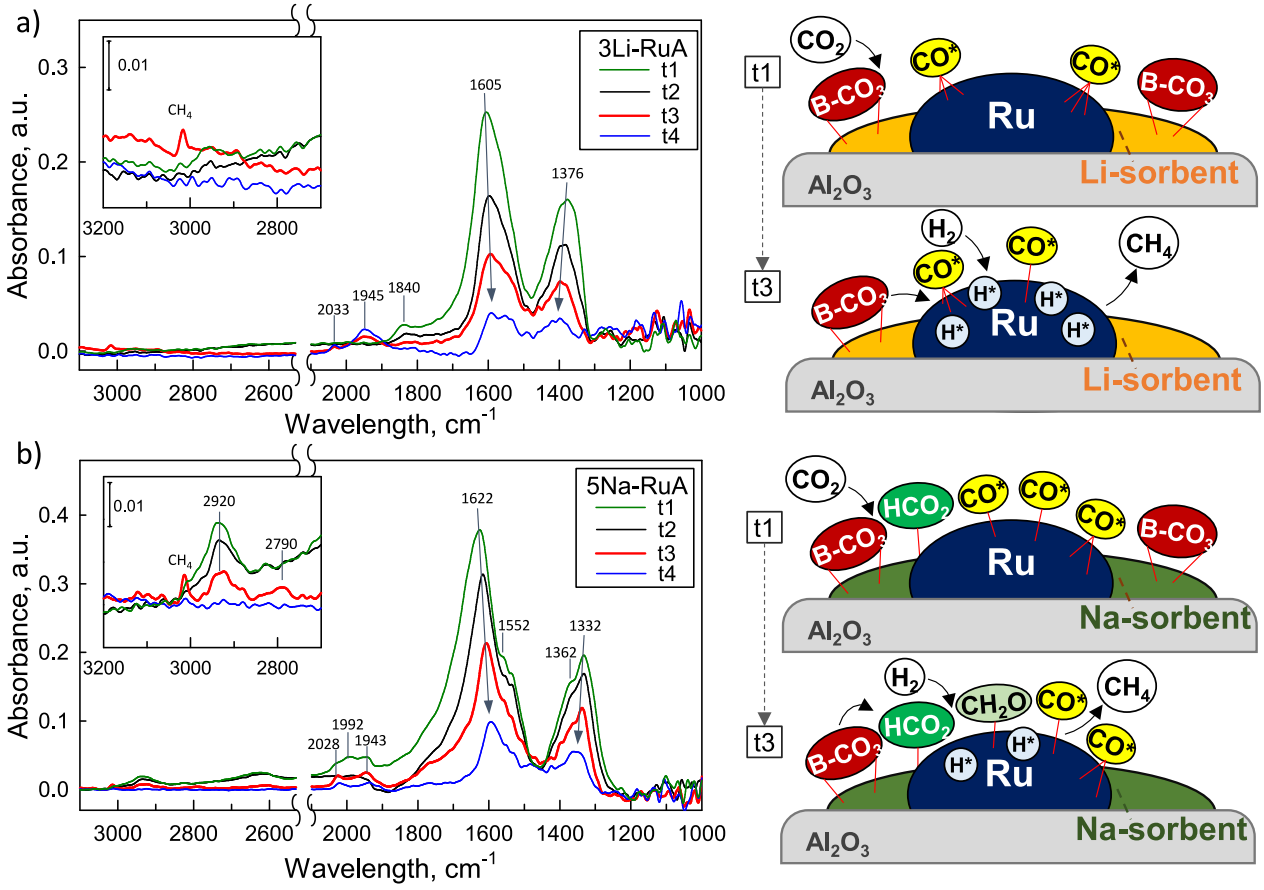

Fig. 8. Time-resolved DRIFT spectra and corresponding schematic representation of the main ad-species at characteristic times during the ICCM operated at 280 °C over (a) 3Li-RuA and (b) 5Na-RuA DFMs: (t1) at the end of CO_2 adsorption, (t2) after purging, (t3) after 1 min and (t4) 14 min of methanation. DFMs pretreated at 360 °C under 2 % H_2 in N_2. Feed sequence: 15 % CO_2 in N_2, 10 min; inert purge, 15 min; 2 % H_2 in N_2, 20 min. Experimental details can be found in Section 2.2. Legend: B-CO_3 = bidentate carbonates; HCO_2 = formates; CH_2O=methoxy; CO*=linear, bridged, multi-bridged carbonyls; H*= hydrogen atom.

intermediates, whereas formates (also detected in small amounts) were only spectators. However, the strong basic character of the support achieved upon Na addition promoted the formation of formates at the interface with metal nanoparticles that became the true reaction intermediates and were ultimately transformed into methane (and water) by the progressive H addition [29,38]. This shift in the reaction mechanism caused a much larger apparent reaction order for the methanation of CO_2 with respect to H_2 [38]. Although the two main reaction pathways are generally regarded as alternatives, depending on the type of support, presence of different promoters and reaction temperature, they can also be involved in a combined reaction scheme [35,38] wherein formates react with H_2 via the RWGS to form more Ru carbonyls [40], which are finally hydrogenated to CH_4.

Eventually, it is worth remarking that the 5Na-RuA and the mixed 3Na3Li-RuA DFMs displayed very similar DRIFTS bands with an analogue temporal evolution during cycles. It can be argued that when both Li and Na were sequentially dispersed (in this specific order and loading) on the surface of the Ru-Al_2O_3 catalyst the impact of sodium prevailed. In particular, the methanation reaction was kinetically inhibited by the high carbonaceous coverages stabilized at the interface between Ru and Na: the consequent decrease of surface hydrogen concentration [28] justifies the higher (2x) apparent reaction order with respect to H_2 measured over 3Na3Li-RuA rather than 3Li-RuA (1.0–1.1 vs 0.45–0.48). It is concluded the number and nature of the adsorbent sites close to catalytic sites must be considered major factors affecting DFM performance requiring careful optimization of both alkali type, loading and deposition strategy [41].

4. Conclusions

Novel dual function materials for Integrated CO_2 Capture and Methanation were developed by dispersing Li and Na (from nitrate precursors) onto a 1 % Ru/Al_2O_3 catalyst aiming to enhance CO_2 capture capacity while maintaining fast methanation activity and minimizing the use of critical raw materials like Ru and Li. TG-MS and time-resolved DRIFTS CO_2 adsorption experiments over combined Li/Na and single Li- or Na-DFMs showed a fast chemisorption mostly forming similar bidentate carbonates on both Na and Li basic-sites. H_2-TPSR results indicated that mixed Na/Li formulations outperform the Na-only counterpart with similar CO_2 capacity in activating the catalytic methanation of pre-adsorbed CO_2 and requiring lower temperatures for complete reactive regeneration of adsorption sites. However, catalytic kinetic studies revealed that Na negatively affects the catalytic activity and selectivity of methanation on the Li-RuA DFM, impacting the apparent reaction orders on CO_2 and H_2. Operando DRIFTS analysis confirmed that Na alters the catalytic mechanism, causing a higher coverage of Ru nanoparticles by carbon species and stabilizing formate/methoxy species as reaction intermediates to methane, in addition to linear and bridged carbonyls, which were the only species detected in the case of Li-RuA. This caused a slower methanation rate over mixed NaLi-Ru/A DFMs compared to pure Li-RuA, requiring higher temperatures (up to 360 °C vs ca 280 °C) and/or longer reaction times to fully utilize their enhanced CO_2 capacity during ICCM cycles in the fixed bed reactor.

These findings can guide the design of optimized DFMs with finely tuned CO_2-sorbent formulations and adsorption strength matching process temperatures, promoting fast hydrogenation kinetics to enhance productivity. This requires maximizing the catalyst-adsorbent interface while preserving free those specific Ru sites where the hydrogenation to methane can proceed promptly. Notably, Lithium emerges as the preferred sorbent phase for Ru/Al_2O_3-based DFMs targeting low-temperature ICCM applications like Direct Air Capture and temperature-swing operation.

Funding

This research was funded by the European Union – NextGeneration EU from the Italian Ministry of Environment and Energy Security POR H_2 AdP MMES/ENEA with involvement of CNR and RSE, PNRR – Mission 2, Component 2, Investment 3.5 “Ricerca e sviluppo sull’idrogeno”, CUP: B93C22000630006.

E.M. Cepollaro acknowledges funding from the European Union – NextGenerationEU under the National Recovery and Resilience Plan (NRRP), Mission 4 Component 2 Investment 3.1, Project Code: IR0000027 – CUP:B33C22000710006 – iENTRANCE@ENL: Infrastructure for Energy TRAnsition aNd Circular Economy @ EuroNanoLab.

In memoriam

On April 2024 our co-author, friend and colleague Dr. Francesco Frusteri suddenly passed away. We would like to pay a tribute to his remarkable contributions to the heterogeneous catalysis community as a committed researcher and distinguished scientist. To many of us he was a desired companion of scientific and social life of conferences and congresses.

Declaration of competing interest

The authors declare that they have no known competing financial interests or personal relationships that could have appeared to influence the work reported in this paper.

Data availability

Data will be made available on request.

Appendix A. Supplementary data

Supplementary data to this article can be found online at https://doi.org/10.1016/j.seppur.2024.129101.

References

[1] J. Mertens, C. Breyer, K. Arning, A. Bardow, R. Belmans, A. Dibenedetto, S. Erkman, J. Gripekoven, G. Léonard, S. Nizou, D. Pant, A.S. Reis-Machado, P. Styring, J. Vente, M. Webber, C.J. Sapart, Carbon capture and utilization: more than hiding CO_2 for some time, Joule (2023) 1–8, https://doi.org/10.1016/j.joule.2023.01.005.

[2] A.D.N. Kamkeng, M. Wang, J. Hu, W. Du, F. Qian, Transformation technologies for CO_2 utilisation: current status, challenges and future prospects, Chemical Engineering Journal 409 (2021) 128138, https://doi.org/10.1016/j.cej.2020.128138.

[3] C. Wu, Q. Huang, Z. Xu, A.T. Sipra, N. Gao, L.P. de Souza Vandenberghe, H. Zhou, A comprehensive review of carbon capture science and technologies, Carbon Capture, Science Technolgy 100178 (2023), https://doi.org/10.1016/j.ccst.2023.100178.

[4] S. Saeidi, S. Najari, V. Hessel, K. Wilson, F.J. Keil, P. Concepción, S.L. Suib, A. E. Rodrigues, Recent advances in CO_2 hydrogenation to value-added products — Current challenges and future directions, Prog. Energy Combust. Sci. 85 (2021) 100905, https://doi.org/10.1016/j.pecs.2021.100905.

[5] G. Liu, S. Sun, H. Sun, Y. Hang, J. Lv, Y. Wang, J. Zeng, Z. Yan, C. Wu, Integrated CO_2 capture and utilisation: a promising step contributing to carbon neutrality, carbon capture, Science Technolgy 100116 (2023), https://doi.org/10.1016/j.ccst.2023.100116.

[6] I.S. Omodolor, H.O. Otor, J.A. Andonegui, B.J. Allen, A.C. Alba-Rubio, Dual-function materials for CO_2 capture and conversion: a review, Ind. Eng. Chem. Res. 59 (2020) 17612–17631, https://doi.org/10.1021/acs.iecr.0c02218.

[7] Y. Chen, L. Shen, L. Chen, Sensitivity study of integrated carbon capture and methanation process using dual function materials, Separation and Purification Technology 344 (2024) 127170, https://doi.org/10.1016/j.seppur.2024.127170.

[8] S. Sun, H. Sun, P.T. Williams, C. Wu, Recent advances in integrated CO_2 capture and utilization: a review, Sustain, Energy Fuels. 5 (2021) 4546–4559, https://doi.org/10.1039/d1se00797a.

[9] L.-P. Merkouri, T.R. Reina, M.S. Duyar, Closing the carbon cycle with dual function materials, Energy & Fuels. 35 (24) (2021) 19859–19880, https://doi.org/10.1021/acs.energyfuels.1c02729.

[10] Y. Zhang, S. Zhao, L. Li, J. Feng, K. Li, Z. Huang, H. Lin, Integrated CO_2 capture and utilization: a review of the synergistic effects of dual function materials, Catal. Sci & Tech. 14 (2024) 790–819, https://doi.org/10.1039/D3CY01289A.

[11] Z. Lv, H. Du, S. Xu, T. Deng, J. Ruan, C. Qin, Techno-economic analysis on CO_2 mitigation by integrated carbon capture and methanation, Applied Energy 355 (2024) 122242, https://doi.org/10.1016/j.apenergy.2023.122242.

[12] M. Abdallah, R. Farrauto, A perspective on bridging academic research and advanced testing on a path towards pilot plant implementation: a case study of integrating CO_2 capture and catalytic conversion with dual function materials, Catal. Today 423 (2022) 113923, https://doi.org/10.1016/j.cattod.2022.10.005.

[13] M.A. Arellano-Treviño, Z. He, M.C. Libby, R.J. Farrauto, Catalysts and adsorbents for CO_2 capture and conversion with dual function materials: Limitations of Ni-containing DFMs for flue gas applications, J. CO_2 Util. 31 (2019) 143–151, https://doi.org/10.1016/j.jcou.2019.03.009.

[14] C. Jeong-Potter, M. Abdallah, C. Sanderson, M. Goldman, R. Gupta, R. Farrauto, Dual function materials (Ru+Na_2O/Al_2O_3) for direct air capture of CO_2 and in situ catalytic methanation: the impact of realistic ambient conditions, Appl. Catal. b: Environ. 307 (2022) 120990, https://doi.org/10.1016/j.apcatb.2021.120990.

[15] A. Bermejo-López, B. Pereda-Ayo, J.A. González-Marcos, J.R. González-Velasco, Mechanism of the CO2 storage and in situ hydrogenation to CH_4. Temperature and adsorbent loading effects over Ru-CaO/Al_2O_3 and Ru-Na_2CO_3/Al_2O_3 catalysts, Appl. Catal. b: Environ. 256 (2019) 117845, https://doi.org/10.1016/J.APCATB.2019.117845.

[16] C. Jeong-Potter, A. Porta, R. Matarrese, C.G. Visconti, L. Lietti, R. Farrauto, Ageing study of low Ru loading dual function materials (DFM) for combined power plant effluent CO_2 capture and methanation, Appl. Catal. b: Environ. 310 (2022) 121294, https://doi.org/10.1016/j.apcatb.2022.121294.

[17] A. Bermejo-López, B. Pereda-Ayo, J.A. Onrubia-Calvo, J.A. González-Marcos, J. R. González-Velasco, Aging studies on dual function materials Ru/Ni-Na/Ca- Al_2O_3 for CO_2 adsorption and hydrogenation to CH_4, J. Environ. Chem. Eng. 10 (2022) 107951, https://doi.org/10.1016/j.jece.2022.107951.

[18] S. Cimino, E.M. Cepollaro, L. Lisi, Sulfur tolerance and self-regeneration mechanism of Na-Ru/ Al_2O_3 dual function material during the cyclic CO_2 capture and catalytic methanation, Appl. Catal. b: Environ. 317 (2022) 121705, https://doi.org/10.1016/j.apcatb.2022.121705.

[19] A. Porta, R. Matarrese, C.G. Visconti, L. Castoldi, L. Lietti, Storage Material Effects on the performance of Ru-Based CO_2 capture and methanation dual functioning materials, Ind. Eng. Chem. Res. 60 (2021) 6706–6718, https://doi.org/10.1021/acs.iecr.0c05898.

[20] S. Cimino, F. Boccia, L. Lisi, Effect of alkali promoters (Li, Na, K) on the performance of Ru/Al_2O_3 catalysts for CO_2 capture and hydrogenation to methane, J. CO_2 Util. 37 (2020) 195–203. doi: 10.1016/j.jcou.2019.12.010.

[21] S. Cimino, E.M. Cepollaro, L. Lisi, Ageing study of Li-Ru/ Al_2O_3 dual function material during the integrated CO_2 capture and methanation with SO_2-containing flue gas, Carbon Capture Science & Technology 6 (2023) 100096, https://doi.org/10.1016/j.ccst.2022.100096.

[22] S. Cimino, R. Russo, L. Lisi, Insights into the cyclic CO_2 capture and catalytic methanation over highly performing Li-Ru/Al_2O_3 dual function materials, Chem. Eng. J. 428 (2022) 131275, https://doi.org/10.1016/j.cej.2021.131275.

[23] A. Bermejo-López, B. Pereda-Ayo, J.A. Onrubia-Calvo, J.A. González-Marcos, J. R. González-Velasco, Tuning basicity of dual function materials widens operation temperature window for efficient CO_2 adsorption and hydrogenation to CH_4, J. CO_2 Util. 58 (2022) 101922, https://doi.org/10.1016/j.jcou.2022.101922.

[24] S. Cimino, E.M. Cepollaro, M. Pazzi, L. Lisi, Sulphur poisoning and regeneration of Li-Ru/ Al_2O_3 dual function material for the integrated CO_2 capture and methanation, Catal. Today 426 (2024) 114366, https://doi.org/10.1016/j.cattod.2023.114366.

[25] J.F.M. Simons, T.J. de Heer, R.C.J. van de Poll, V. Muravev, N. Kosinov, E.J. M. Hensen, Structure Sensitivity of CO_2 Hydrogenation on Ni Revisited, J. Amer. Chem. Soc. 145 (2023) 20289–20301, https://doi.org/10.1021/jacs.3c04284.

[26] L. Falbo, C.G. Visconti, L. Lietti, J. Szanyi, The effect of CO on CO_2 methanation over Ru/ Al_2O_3 catalysts: a combined steady-state reactivity and transient DRIFT spectroscopy study, Appl. Catal. b: Environ. 256 (2019) 117791, https://doi.org/10.1016/j.apcatb.2019.117791.

[27] S.J. Park, X. Wang, M.R. Ball, L. Proano, Z. Wu, C.W. Jones, CO_2 methanation reaction pathways over unpromoted and $NaNO_3$-promoted Ru/Al_2O_3 catalysts, Catal. Sci. & Tech. 12 (2022) 4637–4652, https://doi.org/10.1039/D2CY00515H.

[28] L. Falbo, M. Martinelli, C.G. Visconti, L. Lietti, C. Bassano, P. Deiana, Kinetics of CO_2 methanation on a Ru-based catalyst at process conditions relevant for Power-to-Gas applications, Appl. Catal. b: Environ. 225 (2018) 354–363, https://doi.org/10.1016/J.APCATB.2017.11.066.

[29] L. Proaño, E. Tello, M.A. Arellano-Trevino, S. Wang, R.J. Farrauto, M. Cobo, In-situ DRIFTS study of two-step CO_2 capture and catalytic methanation over Ru, "N_a2O"/A_l2_O3 Dual Functional Material, Appl. Surf. Sci. 479 (2019) 25–30, https://doi.org/10.1016/j.apsusc.2019.01.281.

[30] K. Coenen, F. Gallucci, B. Mezari, E. Hensen, M. van Sint Annaland, An in-situ IR study on the adsorption of CO_2 and H_2O on hydrotalcites, J. CO_2 Util. 24 (2018) 228–239, https://doi.org/10.1016/j.jcou.2018.01.008.

[31] L. Merkouri, J.L. Martín-Espejo, L.F. Bobadilla, J.A. Odriozola, A. Penkova, T. Ramirez Reina, M.S. Duyar, Unravelling the CO_2 capture and conversion mechanism of a NiRu–Na_2O switchable dual-function material in various CO_2 utilisation reactions, J. Mater. Chem. A 11 (2019) 13209–13216, https://doi.org/10.1039/D3TA01892J.

[32] J. Szanyi, J.H. Kwak, Dissecting the steps of CO_2 reduction: 1. The interaction of CO and CO_2 with γ-Al_2O_3: An in situ FTIR study, Physical Chemistry Chemical Physics 16 (2014) 15117–15125, https://doi.org/10.1039/c4cp00616j.

[33] K. Zhao, L. Wang, M. Calizzi, E. Moioli, A. Züttel, In Situ Control of the adsorption species in CO $_2$ hydrogenation: determination of intermediates and Byproducts, The Journal of Physical Chemistry C 122 (2018) 20888–20893, https://doi.org/10.1021/acs.jpcc.8b06508.

[34] S. Jo J.H. Woo T. Nguyen J.E. Kim T.Y. Kim H.J. Ryu B. Hwang J.C. Kim S.C. Lee K. L. Gilliard-AbdulAziz K. l., Zr-Modified Ni/CaO Dual Function Materials (DFMs) for Direct Methanation in an Integrated CO_2 Capture and Utilization Process Energy & Fuels 37 2023 19680 19694 10.1021/acs.energyfuels.3c02935.

[35] A. Porta, R. Matarrese, C.G. Visconti, L. Lietti, Investigation of DFMs for CO_2 capture and methanation by coupled microreactor experiments and FT-IR Spectroscopy, Energy & Fuels 37 (2023) 7280–7290, https://doi.org/10.1021/acs.energyfuels.3c00443.

[36] J. Ilsemann, M.M. Murshed, T.M. Gesing, J. Kopyscinski, M. Bäumer, On the support dependency of the CO2methanation - decoupling size and support effects, Catal. Sci. Tech. 11 (12) (2021) 4098–4114, https://doi.org/10.1039/d1cy00399b.

[37] X. Wang, Y. Hong, H. Shi, J. Szanyi, Kinetic modeling and transient DRIFTS–MS studies of CO2 methanation over Ru/Al_2O_3 catalysts, J. Catal. 343 (2016) 185–195, https://doi.org/10.1016/j.jcat.2016.02.001.

[38] A. Solis-Garcia, T.A. Zepeda, J.C. Fierro-Gonzalez, Spectroscopic evidence of surface species during CO_2 methanation catalyzed by supported metals: A review, Catal. Today 394–396 (2021) 2–12, https://doi.org/10.1016/j.cattod.2021.10.015.

[39] A. Solis-Garcia, J.F. Louvier-Hernandez, A. Almendarez-Camarillo, J.C. Fierro-Gonzalez, Participation of surface bicarbonate, formate and methoxy species in the carbon dioxide methanation catalyzed by ZrO2-supported Ni, Appl. Catal. b: Environ. 218 (2017) 611–620, https://doi.org/10.1016/j.apcatb.2017.06.063.

[40] P. Panagiotopoulou, D.I. Kondarides, X.E. Verykios, Mechanistic aspects of the selective methanation of CO over Ru/TiO2 catalyst, Catal. Today 181 (1) (2012) 138–147, https://doi.org/10.1016/j.cattod.2011.05.030.

[41] L. Merkouri, A.I. Paksoy, T. Ramirez Reina, M.S. Duyar, The need for flexible chemical synthesis and how dual-function materials can pave the way, ACS Catalysis 13 (11) (2023) 7230–7242, https://doi.org/10.1021/acscatal.3c00880.